ACS OMEGA

http://pubs.acs.org/journal/acsodf

Article

Impact of Defects for AlN Single Crystal Thin Film by Metal Nitride Vapor Phase Epitaxy

Luxiao Xie, Hui Zhang, Xinjian Xie, Endong Wang, Xiangyu Lin, Yuxuan Song, Guodong Liu, and Guifeng Chen*

Cite This: *ACS Omega* 2022, 7, 41100−41106

Read Online

ACCESS | Metrics & More | Article Recommendations

ABSTRACT: Herein, the defect-related properties of an AlN sample prepared based on the optimal process parameters by metal nitride vapor phase epitaxy (MNVPE) were investigated. The FWHM values of the (0002)/(10$\bar{1}$2) planes of the sample by MNVPE are 397/422 arcsec; the advantages of similar FWHM values of (0002) and (10$\bar{1}$2) planes will have a huge advantage over other preparation methods such as MOCVD. From the cross-sectional TEM images of the AlN sample, it is found that the fusion of a large number of a + c type dislocations occur at the interface of the low temperature buffer layer and the epitaxial layer, which affects the growth mode of the epitaxial layer. The lower FHWM value of the E_2(high) peak of the Raman spectrum, the lower the point defect concentration, which made the sample gain higher energy defect emission bands in the PL spectra and higher transmittance in the UV−vis transmission spectrum.

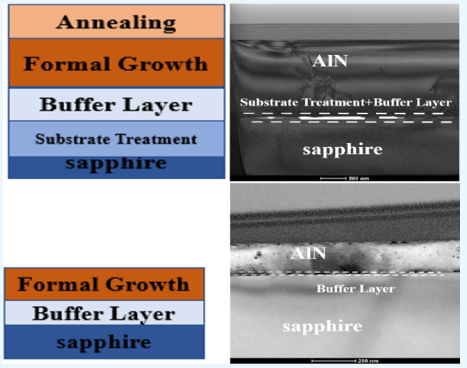

INTRODUCTION

In recent years, with the global spread of COVID-19, sterilization has become a part of people's daily life. As the material with the largest band gap in the III−V group (the band gap is 6.2 eV[1] at room temperature), AlN has great application potential in the field of disinfection and sterilization in the deep ultraviolet field.[2,3] In addition, AlN also has many other physical performance advantages, such as very high thermal conductivity (3.20 $W{\cdot}cm^{-1}{\cdot}K^{-14}$), high piezoelectric coefficient (4.9−5.1 $pm{\cdot}V^{-15}$), high radiation resistance,[4,6,7] etc. Among them, the most potential is that due to the greater thermal conductivity and critical electric field of AlN, AlN devices are likely to surpass current GaN devices in the field of high-voltage devices, AlN or AlGaN with high aluminum content can withstand higher voltages, currents, and temperatures than Si or SiC.

At present, the main problem hindering the development of AlN-based deep ultraviolet light source devices and high-voltage power electronic devices is the inability to obtain native AlN substrates with high crystalline quality and large area. Therefore, there have been a large number of methods for preparing single crystal AlN materials, such as metal organic chemical vapor deposition (MOCVD),[8,9] hydride vapor phase epitaxy (HVPE),[10−12] physical vapor transport (PVT),[13,14] MNVPE,[15−17] etc. Among them, the equipment used in the MOCVD method has been widely used for many years, and the process has been relatively mature; however, due to the fact that the slow growth rate and the inevitable carbon pollution limit large-scale applications, the MNVPE method is essentially a chemical vapor deposition method in which Al vapor reacts with N_2 to directly deposit and grow a single crystal AlN thin film on a sapphire substrate, while the PVT method is a purely physical sublimation process and has the advantages of a fast growth rate and environmental friendliness, but due to the late start of research, its growth mechanism and defect evolution mechanism are still in the initial stage.

EXPERIMENTAL SECTION

The MNVPE setup consists of a rotating graphite subsector heated by induction in a vertical water-cooled cold-wall reactor working at low pressure. Two independently controllable temperature zones exist, in which one is for heating the aluminum source (source zone) and the other one for growing AlN (growth zone). Al vapor was generated in the source zone by heating Al metal and transferred to the growth zone by Ar gas (purity 99.999%). As summarized in Figure 1, the preparation of sample S1 generally needs to go through the following four processes: first, for the substrate pretreatment process, the source zone was maintained at 1200 °C for 10 min to provide sufficient Al vapor, while the growth zone was

Received: July 21, 2022
Accepted: September 26, 2022
Published: November 3, 2022

https://doi.org/10.1021/acsomega.2c04626
ACS Omega 2022, 7, 41100−41106

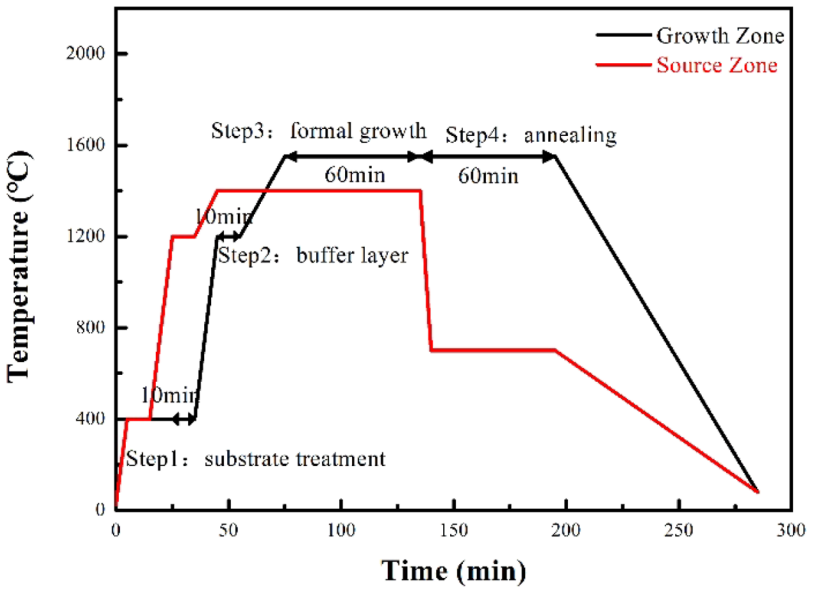

Figure 1. Flow chart of temperature and time for sample S1.

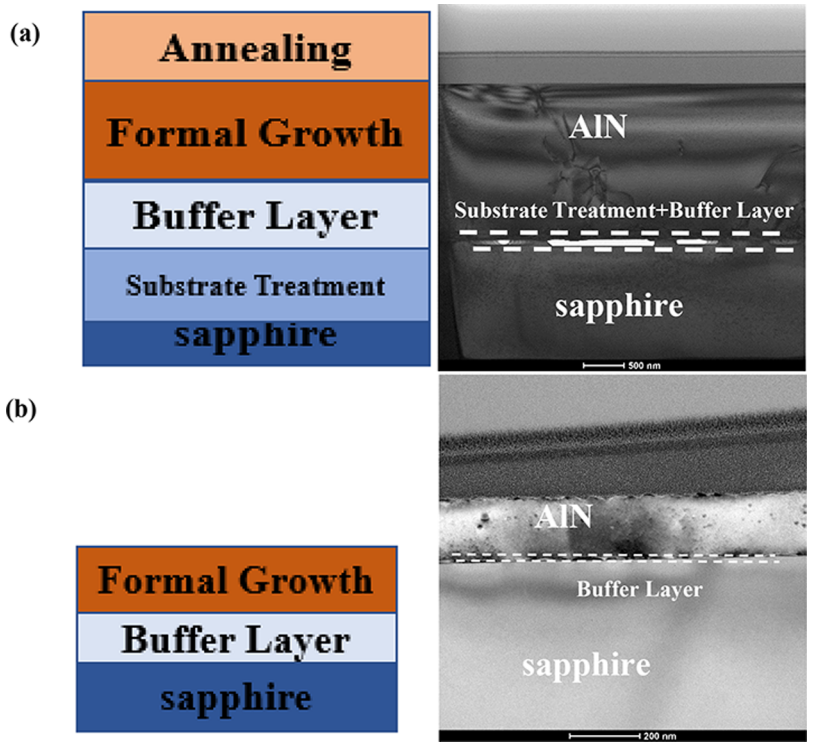

Figure 2. Schematic structure of the AlN sample growth on sapphire substrates and TEM cross section: (a) sample S1; (b) sample S2.

initially heated from room temperature to 400 °C; next, for the low temperature buffer layer process, the source zone was maintained at 1400 °C, while the growth zone was heated from 400 to 1200 °C for 10 min and the reactor pressure was reduced to 10 kPa; afterward, for the formal growth process, the temperature of the growth zone was then raised to 1550 °C and the gas flow rate was set to the growth value for 1 h; finally, for the annealing process, the Ar flow was stopped, and the substrate was heated under a N_2 atmosphere for 1 h at the growth temperature, while sample S2 was obtained by the commonly used MOCVD method with the common process parameters.[9,18,19]

The sample morphologies were characterized atomic force microscopy (AFM, Bruker MultiMode8). The Raman spectra were obtained using the LabRAM HR Evolution system (Horiba Jobin Yvon) at room temperature with a 532 nm solid laser as the excitation source. The X-ray diffraction (XRD) patterns were collected by a Bruker diffractometer (D8 FOUCUS) with Cu Kα radiation. The cross-sectional TEM images were obtained by a transmission electron microscope (JEM-2100F). The optical properties of the AlN layers were examined via photoluminescence (PL) measurements at room temperature with a 325 nm laser as the excitation source and

https://doi.org/10.1021/acsomega.2c04626
ACS Omega 2022, 7, 41100−41106

UV−vis transmission spectra by the UV−vis spectrophotometer (Hitachi U-3900).

DISCUSSION

Figure 2 illustrates the schematic structure of the AlN sample growth on sapphire substrates and TEM cross section, sample S1 was formally grown by the MNVPE method for 1 h. The thickness was about 2 μm in Figure 2a, corresponding to a growth rate of 2 μm/h, while sample S2 was officially grown by the more mature MOCVD method for 1 h, and the thickness was about 200 nm in Figure 2b, corresponding to a growth rate of 0.2 μm/h, which was considered to be 10 times lower than the MNVPE method. The surface morphology of the two samples was investigated by AFM and is shown in Figure 3. As shown in Figure 3a, atomically flat surfaces of AlN with straight parallel steps and terraces are observed for sample S1,which are similar to the microscopic surface of common HVPE,[20] indicating the growth patterns of 2D layered stacks by the MNVPE method, and the AlN tiny islands would coalesce for sample S2 by the MOCVD method, resulting in a step-island surface morphology in Figure 3b. Due to the difference between the two growth modes for the two samples, the root mean square (RMS) of sample S1 is significantly higher than that of sample S2, reaching 1.22 nm. From the AFM results, similar to the HVPE method, the surface flatness of the AlN epitaxial layer prepared by the MNVPE method is more difficult to control, in which the annealing process and substrate treatment have been added to greatly improve the surface flatness.

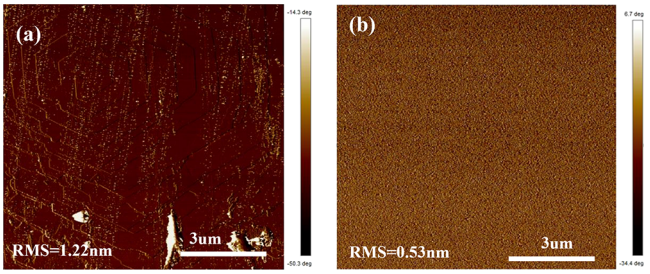

Figure 3. AFM images of the surface morphology and the corresponding roughness (10 × 10 μm): (a) sample S1; (b) sample S2.

The HRXRD rocking curve (XRC) measurements were performed to evaluate the crystal quality of AlN films for different samples. XRC measurements of samples S1 and S2 for the symmetric (0002) plane and asymmetric ($10\bar{1}2$) plane were carried out and are shown in Figure 4. As can be seen from Figure 4, the full width at half-maximums (FWHMs) of the (0002)/($10\bar{1}2$) planes of samples S1 and S2 are 397/422 and 97/359 arcsec, respectively. It is well known that the FWHMs of the (0002) plane and (1012) plane are closely related to the screw dislocation density (N_{screw}) and the edge dislocation density (N_{edge}), respectively.[21−23] It can be seen that the screw dislocation density of sample S1 differs from the edge dislocation density value very slightly, which is a huge advantage over other preparation methods such as MOCVD.[8,9] To further quantitatively evaluate dislocation reduction, an estimation of threading dislocation density (TDD) can be realized by using the empirical formula:

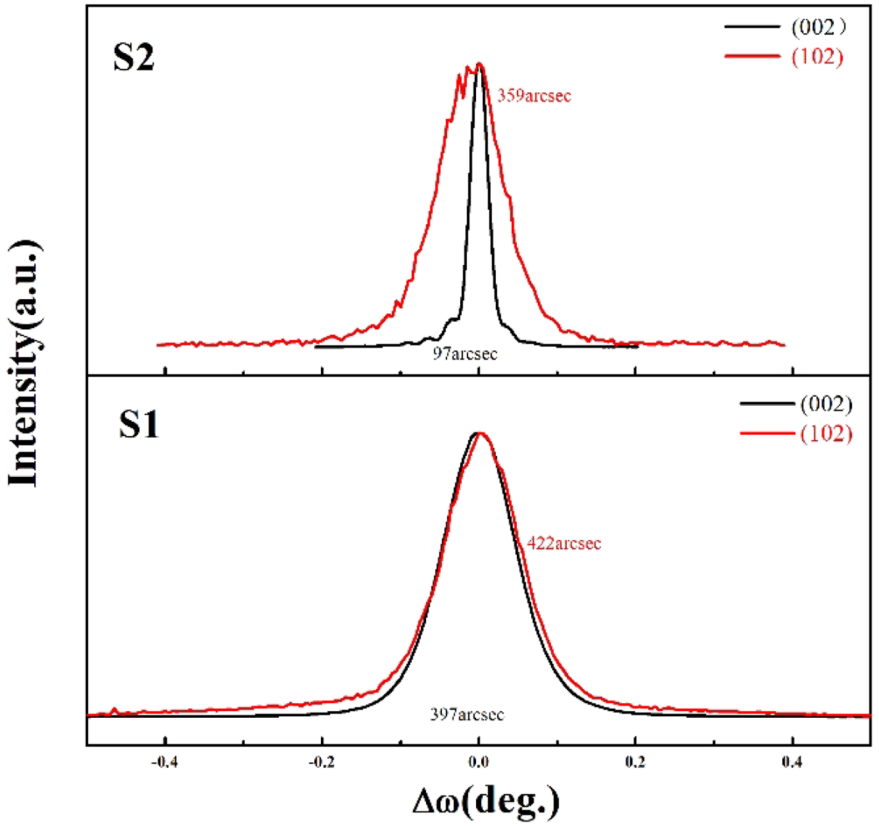

Figure 4. XRC measurements of samples S1 and S2 for the symmetric (0002) plane and asymmetric ($10\bar{1}2$) plane.

https://doi.org/10.1021/acsomega.2c04626
ACS Omega 2022, 7, 41100−41106

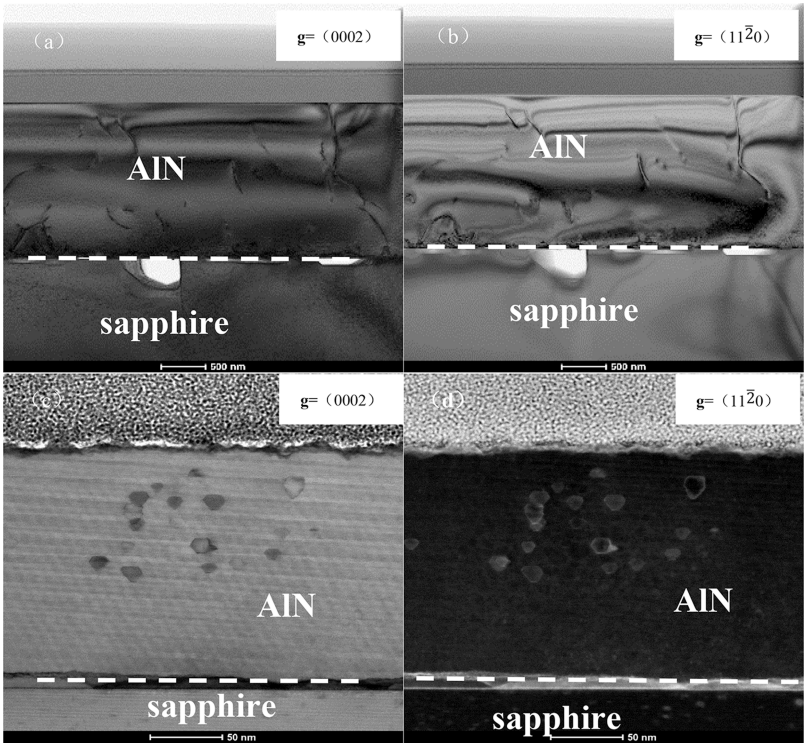

Figure 5. Cross-sectional bright-field TEM images of the AlN samples: (a), (b) S1; (c, d) S2.

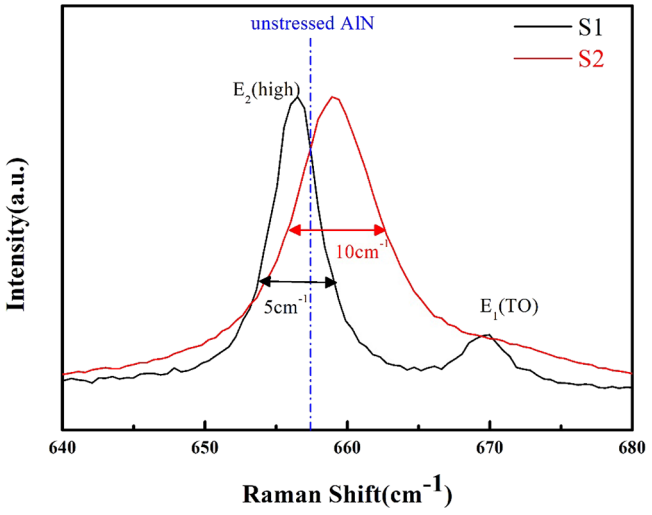

Figure 6. Normalized Raman spectra of the AlN E_2(high) phonon mode.

$$N = \frac{\beta^2}{4.35 \times |\mathbf{b}|}$$

where β is the FWHM value of XRC and **b** is the Burgers vector of corresponding dislocations ($\mathbf{b}_{screw}$= 0.4982 nm, $\mathbf{b}_{edge}$= 0.3112nm[24]). Therefore, the TDDs (including N_{screw} and N_{edge}) in samples S1and S2 can be calculated to be 3.6×10^9 and 1.8×10^9 cm^{-2}, respectively. It can be clearly noticed that the TDD in sample S1 prepared by the MNVPE method is exactly 2 times that of sample S2 prepared by the MOCVD method under the conditions of the best process parameters at present, which indicates that the growth mode plays an important role in controlling the crystal quality. In addition, the advantages of the similar N_{screw} and N_{edge} in the MNVPE method will improve the crystal quality in the future with the continuous reduction of N_{screw}.

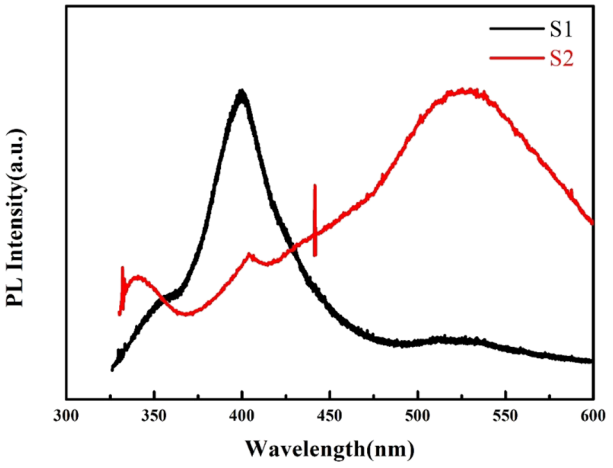

Figure 7. Room temperature PL profiles for AlN samples.

To further study the evolution of dislocations, the cross-sectional TEM images were recorded under two-beam diffraction conditions in the **g** = (0002) and **g** = (11$\bar{2}$0) directions in Figure 5. Generally, there are three types of dislocations in the epitaxial growth of AlN crystal films, namely, a type (edge type), c type (screw type), and a + c type (mixed type). According to the visual principle, when **g** = (0002), only a-type and a + c type dislocations can be seen; when **g** = (11$\bar{2}$0), only c-type and a + c type dislocations can be seen. As shown in Figure 5, most of the dislocations in sample S1 are a + c type dislocations, but obviously, in sample S2, similar to other preparation methods,[10−14] c-type dislocations are significantly more than a-type dislocations. In addition, in sample S1, it can be clearly seen that there are a

https://doi.org/10.1021/acsomega.2c04626
ACS Omega 2022, 7, 41100−41106

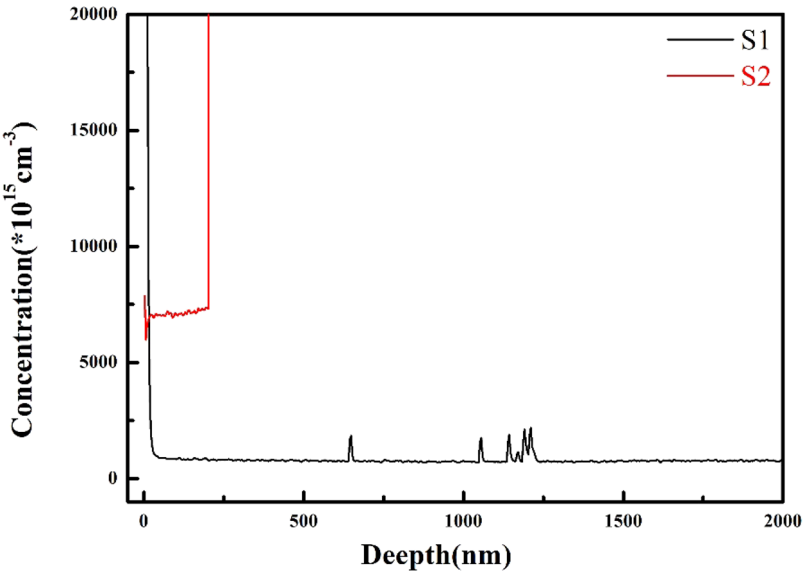

Figure 8. SIMS depth profile of oxygen for samples S1 and S2.

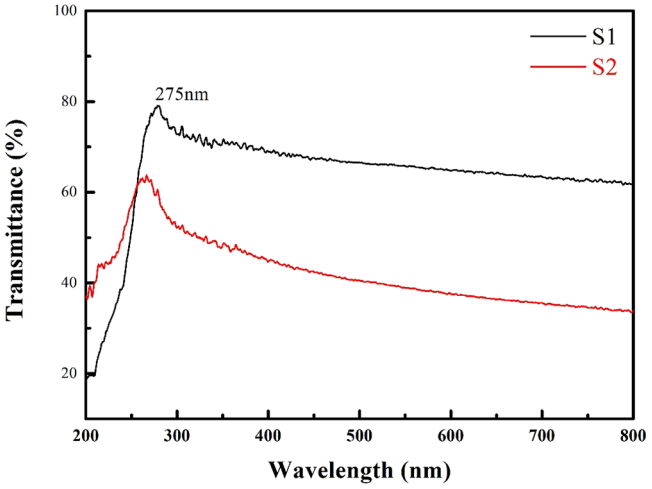

Figure 9. UV−vis transmission spectra of AlN films at room temperature.

large number of a + c type dislocation fusions at the interface between the buffer layer and the epitaxial layer, and a large number of voids of different shapes appear on the sapphire substrate; the growth mode of 3D island-like mergers is changed to that of 2D layered stacks with greatly reduced dislocation density and fast growth rate.

Typical normalized Raman spectra of the AlN E_2(high) phonon mode are shown in Figure 6. V. Lughi and Clarke[25] found that Raman spectroscopy can be used to assess the defect density (mainly point defects) by monitoring the FWHM of the E_2(high) peak. As shown in Figure 6, the FWHM of the E_2(high) peak for sample S1 is 5 cm^{-1}, which is much lower than 10 cm^{-1} of sample S2. Generally, when the FWHM value of the E_2(high) peak is lower than 10 cm^{-1} (the FWHM value of common AlN nanowires[26,27]), it indicates that the integrity of the crystal is better and has fewer defects, so both samples have better crystal quality, but obviously, sample S1 has a lower defect density due to the growth method of the 2D layered stack of the MNVPE method. In addition, since the E_2(high) peak position is highly sensitive to the biaxial strain in the c-plane, the difference between the E_2(high) peak position of the sample and the E_2(high) peak position (657.4 cm^{-1}) of the unstressed AlN sample indicates the magnitude of the residual stress. If the peak position shows red shifts of Raman shift, this is the surface characteristic of the in-plane compressive stress; conversely, if the peak position is blue-shifted, this is the in-plane tensile stress. The in-plane compressive stress was calculated according to the following relationship:

$$\Delta\omega = k\sigma_{xx}$$

where $\Delta\omega$ is the Raman shift of the E_2(high) peak with respect to unstressed AlN and k is the biaxial strain coefficient, 3.7 cm^{-1}/GPa.[28] The residual stresses of samples S1 and S2 are 405 and −243 MPa, respectively. Obviously, the in-plane stress of sample S1 is tensile stress, and the stress value is much lower than that of sample S2. This is because a large number of voids generated by the decomposition of the sapphire substrate at high temperature, and the low temperature buffer layer can release a large amount of thermal stress generated during the cooling process so that the AlN epitaxial layer can grow in a 2D layered stacking mode with a higher rate and lower dislocation.

The PL profiles of samples S1 and S2 are presented in Figure 7. Here, broad luminescence bands are observed at around 400 (3.10 eV) and 525 nm (2.36 eV) and are attributed to the formation of complexes between the nitrogen vacancies (V_N) and oxygen (O) impurities or DX-like shallow donors.[29−32] It can be clearly seen that the relative intensity of the emission band at 400 nm for sample S1 is significantly higher than that at 525 nm, the relative intensity and the width of the emission band at 525 nm are significantly higher than that at emission band at 400 nm for sample S2. As shown in the SIMS depth profile of oxygen for samples S1 and S2 in Figure 8, the O concentration of the AlN epitaxial layer of sample S1 is much lower than that of sample S2, which is completely consistent with the position and intensity of the emission band in the PL spectrum. Obviously, the defect emission band of sample S1 narrows to the high-energy edge, which is due to the fact that fewer point defects (combined with the analysis of the previous Raman spectrum) are more likely to form shallow donor levels, so that the defects are more likely to emit light at low wavelengths (high energy). In order

https://doi.org/10.1021/acsomega.2c04626
ACS Omega 2022, 7, 41100−41106

to further study the effect of point defects on the luminescence properties of AlN samples, the UV−vis transmission spectra were performed for samples S1 and S2 in Figure 9. Apparently, both samples S1 and S2 have a significant peak around 275 nm; the appearance of this peak may be related to the defects related to V_N or the combination of V_N and O[29,30] (according to the other previous optical performance tests on the samples). In addition, both S1 and S2 show high light transmittance; sample S1 obviously has a higher UV transmittance, reaching more than 70%, which is closely related to the lower point defect concentration.

RESULTS

In summary, the AlN sample prepared based on the optimal process parameters by MNVPE has a surface roughness of about 1.22 nm (10 μm × 10 μm) at a growth rate of 2 μm/h, which is slightly higher than that of the samples prepared by MOCVD. From the XRC diffractogram, the FWHM values of the (0002)/(10$\bar{1}$2) planes of the sample by MNVPE are 397/422 arcsec; although this value is higher than that of samples prepared by MOCVD, the advantages of similar FWHM values of (0002) and (10$\bar{1}$2) planes will continue to improve crystal quality in the future. Furthermore, due to the existence of a large number of voids and low-temperature buffer layers on the surface of the sapphire substrate, which affects the growth mode of the epitaxial layer, it is found that the fusion of a large number of a + c type dislocations occur at the interface of the low temperature buffer layer and the epitaxial layer from the cross-sectional TEM images of the AlN sample by MNVPE. Moreover, through the FHWM value of the E_2(high) peak of the Raman spectrum, it is found that the sample prepared by the MNVPE method have a lower point defect concentration than the sample prepared by the MOCVD method, this subsequently is evidenced by higher energy defect emission bands in PL spectra and higher transmittance in the UV−vis transmission spectrum. We firmly believe that with the continuous improvement of the MNVPE method, it will become one of the methods to rapidly prepare high-quality AlN substrates.

AUTHOR INFORMATION

Corresponding Author

Guifeng Chen − *School of Materials Science and Engineering, Hebei University of Technology, Tianjin 300132, China; Hebei Engineering Laboratory of Photoelectronic Functional Crystals, Hebei University of Technology, Tianjin 300130, China*; Phone: +86 13920838656; Email: cgfchen@hebut.edu.cn

Authors

Luxiao Xie − *School of Materials Science and Engineering, Hebei University of Technology, Tianjin 300132, China*; orcid.org/0000-0001-8770-1712

Hui Zhang − *School of Materials Science and Engineering, Hebei University of Technology, Tianjin 300132, China; Hebei Engineering Laboratory of Photoelectronic Functional Crystals, Hebei University of Technology, Tianjin 300130, China*

Xinjian Xie − *School of Materials Science and Engineering, Hebei University of Technology, Tianjin 300132, China*

Endong Wang − *School of Materials Science and Engineering, Hebei University of Technology, Tianjin 300132, China*

Xiangyu Lin − *School of Materials Science and Engineering, Hebei University of Technology, Tianjin 300132, China*

Yuxuan Song − *School of Materials Science and Engineering, Hebei University of Technology, Tianjin 300132, China*

Guodong Liu − *School of Materials Science and Engineering, Hebei University of Technology, Tianjin 300132, China; Hebei Engineering Laboratory of Photoelectronic Functional Crystals, Hebei University of Technology, Tianjin 300130, China*; orcid.org/0000-0002-3173-6462

Complete contact information is available at: https://pubs.acs.org/10.1021/acsomega.2c04626

Author Contributions

All authors contributed equally to this work.

Notes

The authors declare no competing financial interest.

ACKNOWLEDGMENTS

This work was supported by the National Natural Science Foundation of China (grant no. 51871089), S&T Program of Hebei (grant no. 20311001D), the project for Science and Technology Correspondent of Tianjin City (grant no. 20YDTPJC01710), and the Research Foundation of Education Bureau of Hebei (grant no. QN2021044).

REFERENCES

(1) Gadenne, M.; Plon, J.; Gadenne, P. Optical properties of AlN thin films correlated with sputtering conditions. *Thin Solid Films* **1998**, *333*, 251−255.

(2) Sumathi. Status and Challenges in Hetero-epitaxial Growth Approach for Large Diameter AlN Single Crystalline Substrates. *ECS J. Solid State Sci. Technol.* **2021**, *10*, No. 035001.

(3) Miwa, S.; Yano, S.; Hiroshima, Y.; Tome, Y.; Uehara, F.; Mii, S.; Efimova, E. V.; Kimura, H.; Hayashi, K.; Tsuchiya, H.; Hoffman, R. M. Imaging UVC-induced DNA damage response in models of minimal cancer. *J. Cell. Biochem.* **2013**, *114*, 2493.

(4) Jagannadham, K.; Watkins, T. R.; Dinwiddie, R. B. Novel heat spreader coatings for high power electronic devices[J]. *J. Mater. Sci.* **2002**, *37*, 1363−1376.

(5) Lueng, C. M.; Chan, H. L. W.; Fong, W. K.; Surya, C.; Choy, C. L.Piezoelectric coefficients of aluminum nitride and gallium nitride. *MRS Online Proc. Libr.*1999, DOI: 10.1557/PROC-572-389.

(6) Chen, G.; Abou-Galala, F.; Xu, Z.; Sadler, B. M. Experimental evaluation of LED-based solar blind NLOS communication links. *Opt. Express* **2008**, *16*, 15059−15068.

(7) Tsai, D. S.; Lien, W. C.; Lien, D. H.; Chen, K. M.; Tsai, M. L.; Senesky, D. G.; Yu, Y. C.; Pisano, A. P.; He, J. H. Solar-blind photodetectors for harsh electronics. *Sci. Rep.* **2013**, *3*, 1.

(8) Tang, B.; Hu, H.; Wan, H.; Zhao, J.; Zhou, S. Growth of high-quality AlN films on sapphire substrate by introducing voids through growth-mode modification. *Appl. Surf. Sci.* **2020**, *518*, No. 146218.

(9) Huang, J.; Niu, M. T.; Sun, M. S.; Su, X. J.; Xu, K.; Xu, K. Investigation of hydride vapor phase epitaxial growth of AlN on sputtered AlN buffer layers. *CrystEngComm* **2019**, 2431.

(10) Boichot, R.; Claudel, A.; Baccar, N.; Milet, A.; Blanquet, E.; Pons, M. Epitaxial and polycrystalline growth of AlN by high temperature CVD: Experimental results and simulation. *Surf. Coat. Technol.* **2010**, *205*, 1294−1301.

(11) Nikolaev, A.; Nikitina, I.; Zubrilov, A.; Mynbaeva, M.; Melnik, Y.; Dmitriev, V. AlN Wafers Fabricated by Hydride Vapor Phase Epitaxy. *MRS Internet J. Nitride Semicond. Res.* **2000**, *5*, 432−437.

(12) Kumagai, Y.; Yamane, T.; Koukitu, A. Growth of thick AlN layers by hydride vapor-phase epitaxy. *J. Cryst. Growth* **2005**, *281*, 62−67.

(13) Epelbaum, B. M.; Bickermann, M.; Nagata, S.; Heimann, P.; Filip, O.; Winnacker, A. Similarities and differences in sublimation growth of SiC and AlN. *J. Cryst. Growth* **2007**, *305*, 317−325.
(14) Epelbaum, B. M.; Seitz, C.; Magerl, A.; Bickermann, M.; Winnacker, A. Natural growth habit of bulk AlN crystals. *J. Cryst. Growth* **2004**, *265*, 577−581.
(15) Wu, P. T.; Funato, M.; Kawakami, Y. Environmentally friendly method to grow wide-bandgap semiconductor aluminum nitride crystals: Elementary source vapor phase epitaxy. *Sci. Rep.* **2015**, *5*, 17405.
(16) Wu, P. T.; Kishimoto, K.; Funato, M.; Kawakami, Y. Control of Crystal Morphologies and Interface Structures of AlN Grown on Sapphire by Elementary Source Vapor Phase Epitaxy. *Cryst. Growth Des.* **2016**, *16*, 6337−6342.
(17) Kishimoto, K.; Funato, M.; Kawakami, Y. Effects of Al and N2 Flow Sequences on the Interface Formation of AlN on Sapphire by EVPE. *Crystals* **2017**, *7*, 123.
(18) Bo, L.; Zhang, S.; Yin, J. Y.; Zhang, X. W.; Shao-Bo, D.; Feng, Z. H.; Cai, S. J. Effect of high-temperature buffer thickness on quality of AlN epilayer grown on sapphire substrate by metalorganic chemical vapor deposition. *Chin. Phys. B* **2013**, *22*, 449−452.
(19) *UTI-AlN-050A 2″AlN templates.* Retrieved from https://www.utrendtech.com/index.php?route=product/product&path=151&product_id=69.
(20) Jiang, K.; Sun, X.; Ben, J.; Jia, Y.; Liu, H.; Wang, Y.; Wu, Y.; Kai, C.; Li, D. The defect evolution in homoepitaxial AlN layers grown by high-temperature metal−organic chemical vapor deposition. *CrystEngComm* **2018**, 2720.
(21) Eriguchi, K. I.; Hiratsuka, T.; Murakami, H.; Kumagai, Y.; Koukitu, A. High-temperature growth of thick AlN layers on sapphire (0 0 0 1) substrates by solid source halide vapor-phase epitaxy. *J. Cryst. Growth* **2008**, *310*, 4016−4019.
(22) Boichot, R.; Coudurier, N.; Mercier, F.; Lay, S.; Crisci, A.; Coindeau, S.; Claudel, A.; Blanquet, E.; Pons, M. Epitaxial growth of AlN on c-plane sapphire by High Temperature Hydride Vapor Phase Epitaxy: Influence of the gas phase N/Al ratio and low temperature protective layer. *Surf. Coat. Technol.* **2013**, *237*, 118−125.
(23) Liu, J. Q.; Wang, J. F.; Liu, Y. F.; Huang, K.; Hu, X. J.; Zhang, Y. M.; Xu, Y.; Xu, K.; Yang, H. High-resolution X-ray diffraction analysis on HVPE-grown thick GaN layers. *J. Cryst. Growth* **2009**, *311*, 3080−3084.
(24) Zhang, Y.; Long, H.; Zhang, J.; Tan, B.; Chen, Q.; Zhang, S.; Shan, M.; Zheng, Z.; Dai, J.; Chen, C. Fast growth of high quality AlN films on sapphire using a dislocation filtering layer for ultraviolet light-emitting diodes. *CrystEngComm* **2019**, *21*, 4072−4078.
(25) Lughi, V.; Clarke, D. R. Defect and stress characterization of AlN films by Raman spectroscopy. *Appl. Phys. Lett.* **2006**, *89*, 2653.
(26) Zhao, Q.; Zhang, H.; Xu, X.; Wang, Z.; Xu, J.; Yu, D.; Li, G.; Su, F. Optical properties of highly ordered AlN nanowire arrays grown on sapphire substrate. *Appl. Phys. Lett.* **2005**, *86*, 193101.
(27) Lei, M.; Yang, H.; Guo, F. Y.; Song, B.; Li, P. G.; Tang, W. H. Synthesis and optical property of high purity AlN nanowires. *Mater. Sci. Eng., B* **2007**, 85.
(28) Tang, B.; Wan, Z.; Hu, H.; Gong, L.; Zhou, S. Strain management and AlN crystal quality improvement with an alternating V/III ratio AlN superlattice. *Appl. Phys. Lett.* **2021**, *118*, 262101.
(29) Manova, D.; Dimitrova, V.; Fukarek, W.; Karpuzov, D. Investigation of d.c.-reactive magnetron-sputtered AlN thin films by electron microprobe analysis, X-ray photoelectron spectroscopy and polarised infra-red reflection. *Surf. Coat. Technol.* **1998**, *106*, 205−208.
(30) He, J. H.; Yang, R. S.; Chueh, Y. L.; Chou, L. J.; Chen, L. J.; Wang, Z. L. Aligned AlN nanorods with multi-tipped surfaces - Growth, field-emission, and cathodoluminescence properties. *Adv. Mater.* **2006**, *18*, 650.
(31) Zhao, Q.; Feng, S.; Zhu, Y.; Xu, X.; Zhang, X.; Song, X.; Xu, J.; Chen, L.; Yu, D. Annealing effects on the field emission properties of AlN nanorods. *Nanotechnology* **2006**, *17*, S351−S354.
(32) Shen, L.; Cheng, T.; Wu, L.; Li, X.; Cui, Q. Synthesis and optical properties of aluminum nitride nanowires prepared by arc discharge method. *J. Alloys Compd.* **2008**, *465*, 562−566.

https://doi.org/10.1021/acsomega.2c04626
ACS Omega 2022, 7, 41100−41106